

Is Heuristic Sampling Necessary in Training Deep Object Detectors?

Joya Chen, *Student Member, IEEE*, Dong Liu, *Senior Member, IEEE*, Tong Xu, *Member, IEEE*, Shiwei Wu, Yifei Cheng, and Enhong Chen, *Senior Member, IEEE*

Abstract—To train accurate deep object detectors under the extreme foreground-background imbalance, heuristic sampling methods are always necessary, which either re-sample a subset of all training samples (hard sampling methods, *e.g.* biased sampling, OHEM), or use all training samples but re-weight them discriminatively (soft sampling methods, *e.g.* Focal Loss, GHM). In this paper, we challenge the necessity of such hard/soft sampling methods for training accurate deep object detectors. While previous studies have shown that training detectors without heuristic sampling methods would significantly degrade accuracy, we reveal that this degradation comes from an unreasonable classification gradient magnitude caused by the imbalance, rather than a lack of re-sampling/re-weighting. Motivated by our discovery, we propose a simple yet effective *Sampling-Free* mechanism to achieve a reasonable classification gradient magnitude by initialization and loss scaling. Unlike heuristic sampling methods with multiple hyperparameters, our *Sampling-Free* mechanism is fully data diagnostic, without laborious hyperparameters searching. We verify the effectiveness of our method in training anchor-based and anchor-free object detectors, where our method always achieves higher detection accuracy than heuristic sampling methods on COCO and PASCAL VOC datasets. Our *Sampling-Free* mechanism provides a new perspective to address the foreground-background imbalance. Our code will be released at <https://github.com/ChenJoya/sampling-free>.

Index Terms—Object Detection, Foreground-Background Imbalance, Heuristic Sampling Methods

I. INTRODUCTION

WITH the development of deep learning [1], [2], recent years have witnessed remarkable advancement in object detection [3]. Among them, representative successes include two-stage R-CNN detectors [4]–[15]: their first stage uses a region proposal network (RPN [4]) to generate some candidates from dense, predefined bounding-boxes (*i.e.* anchors), then the second stage uses a region-of-interest subnet (RoI-subnet) for object classification and localization. To pursue higher efficiency, one-stage approaches [16]–[23] directly recognize objects from dense anchors rather than generating candidate proposals. Both two-stage and one-stage detectors adopt the anchoring scheme, where massive anchors ($\sim 10^5$) are uniformly sampled over an image.

Corresponding Author: E. Chen.

J. Chen, T. Xu, S. Wu, Y. Cheng, and E. Chen are with Anhui Province Key Lab of Big Data Analysis and Application, School of Computer Science, University of Science and Technology of China. E-mail: {chenjoya, dwustc}@mail.ustc.edu.cn, {tongxu, cheneh}@ustc.edu.cn.

D. Liu is with CAS Key Laboratory of Technology in Geo-Spatial Information Processing and Application System, Department of Electronic Engineering and Information Science, University of Science and Technology of China. E-mail: dongliu@ustc.edu.cn.

Nevertheless, when training these anchor-based detectors, only a few anchors ($\sim 10^2$) that highly overlap with objects will be assigned to foreground samples, which always results in an extreme imbalance between foreground and background (*i.e.* *fg*-*bg* imbalance) within the anchors. In previous studies [17], [24], such imbalance may impede the training from convergence, as well as limit the detection accuracy. More recently, anchor-free object detectors [11], [14], [25]–[33] have gained much attention due to the replacement of anchors by points (*e.g.* corner/center points), but they still suffer from the similar imbalance within the points.

To address the *fg*-*bg* imbalance, several heuristic methods have been proposed to train deep object detectors in recent years. These methods can be divided into two categories. The first category re-samples a subset of training samples, *e.g.* biased sampling [4], online hard example mining [34] (OHEM), IoU-balanced sampling [12]. The second category re-weights training samples discriminatively, *i.e.* assigns different weights to different training samples, like Focal Loss [17], gradient harmonizing mechanism [24] (GHM), prime sample attention mechanism [35] (PISA). According to [36], these two categories can be named “hard sampling methods” and “soft sampling methods,” respectively. We also use the term “heuristic sampling methods” to refer to them in the following.

Although deep object detectors are always equipped with heuristic sampling methods, it is still very difficult to design a suitable hard/soft sampling strategy. Each heuristic sampling methods has a different re-sampling/re-weighting method — as it is unknown which sample and what weighting value is better. For example, in GHM [24], the authors hold the opinion that the optimal distribution of gradient is hard to define and requires further research. Moreover, heuristic sampling methods always introduces multiple hyperparameters, which requires laborious searching.

Can we discard heuristic sampling methods when training deep object detectors? In the past, it was demonstrated [17], [24] that the detector without heuristic sampling methods will suffer from the extreme *fg*-*bg* imbalance, which would trail the detector with heuristic sampling methods about 20% detection accuracy. Some methods [23], [33], [37]–[40] adaptively define foreground/background labels to anchors/points, but they still rely on heuristic sampling methods to address the *fg*-*bg* imbalance. Other ranking-based methods [41]–[43] try to avoid the *fg*-*bg* imbalance by transforming the classification task into the ranking task, but they select pairs of N samples to train, thus have much greater computational cost than heuristic sampling methods ($\mathcal{O}(N^2)$ vs. $\mathcal{O}(N)$). It seems impossible to

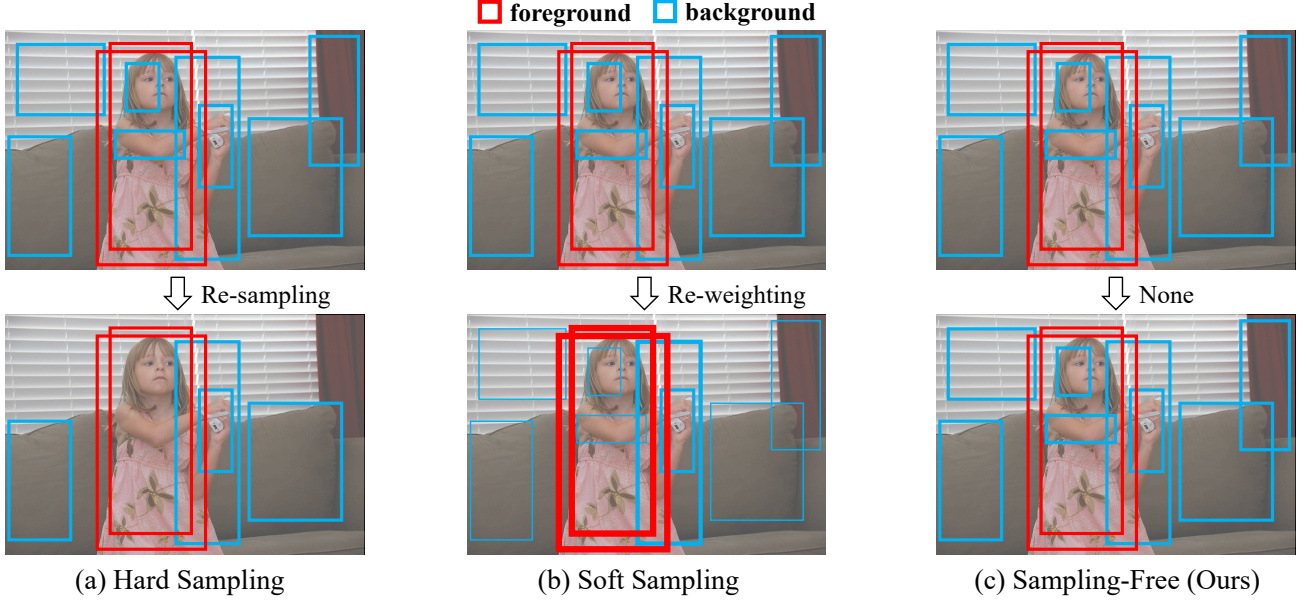


Fig. 1. This figure illustrates the differences between heuristic sampling methods and the Sampling-Free mechanism in the treatment of training samples. (a) Hard sampling (e.g. biased sampling [4], OHEM [34], IoU-balanced sampling [12]) re-samples a subset of training samples; (b) Soft sampling (e.g. Focal Loss [17], GHM [24], PISA [35]) uses all training samples but focuses on some of them by re-weighting. For instance, thicker boxes in (b) denote training samples with higher weights. (c) Sampling-Free equally uses all training samples.

make a cost-free replacement of heuristic sampling methods when training a deep object detector.

In this paper, we discover that a reasonable classification gradient magnitude is the key to address the *fg-bg* imbalance, rather than hard/soft sampling. Motivated by this, we propose a simple yet effective *Sampling-Free* mechanism that adaptively controls the classification gradient magnitude by initialization and loss scaling techniques, which enables discarding heuristic sampling methods but achieves better accuracy. Specifically, at the start of the training, the optimal bias initialization is used to reduce the excessive classification gradient magnitude caused by *fg-bg* imbalance. During the training process, we leverage the bounding-box regression loss to adjust the classification loss, to achieve an adaptive adjustment for the classification gradient magnitude. As shown in Fig. 1, unlike heuristic sampling methods, our method treats all training samples equally, without any hyperparameters introduced.

Experimental results on COCO [44] and PASCAL VOC [45] datasets have demonstrated that our method is effective for both anchor-based and anchor-free object detectors, where Sampling-Free always achieves higher detection accuracy than heuristic sampling methods. By replacing Focal Loss [17] with Sampling-Free in the adaptive label assignment method PAA [39], we obtain a state-of-the-art 49.6 AP on COCO test-dev, without bells and whistles. Sampling-Free is also generalized for the instance segmentation task, which helps Mask R-CNN to obtain better segmentation accuracy. Moreover, there is no hyperparameter introduced in our method. Our Sampling-Free mechanism provides a new perspective to address the *fg-bg* imbalance.

Our main contributions are as follows:

- For the first time, we discover what prevents detectors without heuristic sampling methods from achieving good

accuracy — the unreasonable classification gradient magnitude under the *fg-bg* imbalance, rather than the lack of re-sampling/re-weighting on training samples.

- We propose a novel Sampling-Free mechanism that enables training deep object detectors without heuristic sampling methods. It adaptively controls the classification gradient magnitude by initialization and loss scaling, which is easy to implement and introduces no hyperparameters.

- Collaborating with Sampling-Free mechanism, it is feasible to train deep object detectors without any hard/soft sampling methods and achieve better results on COCO and PASCAL VOC benchmarks.

II. RELATED WORK

Classical object detectors [46], [47] usually rely on hand-crafted feature extractor, which is hard to design. With the development of deep learning [1], [2], deep object detectors quickly come to dominate object detection. In this section, we introduce the development of deep object detectors, then introduce the concept, cause, and solution of the *fg-bg* imbalance. Finally, we discuss the relations and differences between our work and previous works.

A. Deep Object Detection

Among deep object detectors, the anchor-based approach is the most popular approach, which tiles massive default bounding-boxes (*i.e.* anchors) on an image to cover objects. There are mainly two types of anchor-based approaches:

- 1) *Two-stage Anchor-based*: It is popularized by Faster R-CNN [4], which firstly generates some candidates from massive anchors by region proposal network (RPN [4]), then determines the accurate location and object category by a

subnetwork (RoI-subnet [48], [49]). A large number of Faster R-CNN variants [5]–[15] appear over the years, yielding a large improvement in detection accuracy.

2) *One-stage Anchor-based*: It is popularized by SSD [50], which performs much faster than two-stage detectors due to the elimination of the RPN, but usually achieves lower accuracy than two-stage detectors. A series of advances [16]–[23], [40] in recent years promote one-stage anchor-based detector to be more accurate.

In recent years, a large number of anchor-free approaches are proposed, which detect objects by points or regions rather than anchors. Most anchor-free object detectors follow the one-stage detection pipeline but eliminate the usage and hyper-parameters of “anchor boxes”, which shows better simplicity. Although the differences among anchor-free detectors are much smaller than the differences between one-stage and two-stage anchor-based detectors, there are some subtle differences in the definition of training samples among different anchor-free detectors. Specifically, some of the anchor-free detectors detect objects by generating bounding-boxes from pre-defined or self-learned keypoints. The early attempt of pre-defined points is CornerNet [25], which uses the top-left corner and bottom-right corner to represent objects. After that, researchers use various pre-defined points to represent objects, such as extreme points [26], grid points [11], center points [27], [28], and self-learned points [29], [30]. Others [14], [31]–[33] try to learn the position of the object center, and then regress the distances from the center to the four sides of the object bounding-box for detection. The most popular center-based anchor-free detector is FCOS [31], which regards all the locations around the center of objects as foreground examples. GA-RPN [14] successfully designs an anchor-free RPN in the two-stage pipeline.

B. Foreground-Background Imbalance Problem

Training a deep object detector involves two tasks: classification and localization. For classification, the number of background examples is much larger than foreground examples, which is known as the *fg-bg* imbalance [17]. We introduce it in the different label assignment strategy:

1) *Fg-bg Imbalance in Fixed Label Assignment*: In the fixed label assignment [4], [25], [31], [50], there is a pre-defined rule to assign a training sample to a *fg/bg* example. For instance, the anchor-based approach usually considers anchors that have large intersection-over-union (IoU) with ground-truths as foreground examples (*e.g.* $\text{IoU} > 0.5$). The anchor-free approach usually regards points around the center as foreground examples. However, the total number of anchors/points is always huge, which may be $10^3 \sim 10^4$ times more than foreground anchors/points. Therefore, during training, the *fg-bg* imbalance inevitably occurs in the classification task.

2) *Fg-bg Imbalance in Adaptive Label Assignment*: Recently, several adaptive label assignment methods [23], [33], [37]–[40] are proposed to overcome the limitations of fixed label assignment. However, they still suffer from extreme *fg-bg* imbalance. For example, FreeAnchor [23] claims that it faces an even more serious sample imbalance than RetinaNet [17].

These methods still rely on Focal Loss [17] to address the *fg-bg* imbalance in the classification task.

C. Solutions for Foreground-Background Imbalance

As we can see, the *fg-bg* imbalance always exists in training deep object detectors, which impedes deep object detectors from achieving higher accuracy as reported in [17], [24]. In previous works, there are three solutions:

1) *Sampling Methods*: It is the most common solution for *fg-bg* imbalance, which has two groups [36] — hard sampling and soft sampling. The hard sampling method re-samples a set of training samples by some strategies. For example, biased sampling [4] randomly samples 256 examples with 1:1 *fg-to-bg* ratio during training RPN. OHEM [34] and IoU-balanced sampling [12] selects training samples according to loss and IoU values, respectively. The objectness [16], [19], [20] modules, generative methods [51], [52] can also be regarded as hard sampling methods. Soft sampling re-weights training samples discriminatively by some strategies. Focal Loss [17] dynamically assigns higher weight to the hard training samples (*i.e.* with high loss value). Similar to Focal Loss, GHM [24] suppresses gradients originating from easy and very hard training samples (*i.e.* with low loss value). PISA [35] re-weights training samples according to the IoU between training samples and ground-truths.

2) *Classification to Ranking*: As the *fg-bg* imbalance always exists in classification task in deep object detectors, AP Loss [41] and DR Loss [42] propose to convert the classification task into ranking task. They consider to train a pair of samples rather than independent sample. Specifically, the predicted score of one training sample is transformed into the difference between the predicted scores of two training samples. These methods are also quite in line with the detection evaluation metric (average precision, AP).

To date, almost all deep object detectors are equipped with sampling methods during training. The ranking task, however, trains pairs of N examples thus has $\mathcal{O}(N^2)$ computational cost, which is much higher than $\mathcal{O}(N)$ cost of the classification task. Although sampling methods are popular, the re-sampling/re-weighting strategy is hard to design, and both sampling methods and ranking-based methods require laborious hyperparameter tuning. Our work overcomes these shortcomings, which discards sampling methods in the classification task without any hyperparameters introduced.

III. INVESTIGATION

Under the *fg-bg* imbalance, training a deep object detector without heuristic sampling methods will lead to a nearly 20% decrease in the detection accuracy. In this section, we will investigate why this is the case. It will be revealed that the decrease should be attributed to the unreasonable gradient magnitude, rather than the lack of re-sampling/re-weighting on training samples. In the following, we first mathematically introduce *fg-bg* imbalance and sampling methods, then theoretically analyze their impact on the training process. Finally, we experimentally demonstrate that the gradient magnitude is the key factor affecting the detector accuracy.

A. Concepts

1) *Foreground-Background Imbalance*: In general, deep object detectors tend to generate numerous samples to cover as many objects as possible. Although there are various label assignment strategies [4], [17], [23], [38], [39] to define foreground and background samples, the imbalance between foreground and background samples will be inevitably caused due to the rarity of objects and the majority of samples, namely foreground-background (*fg-bg*) imbalance. In other words, the number of foreground samples N^f is much smaller than that of background samples N^b (*i.e.* $N^f \ll N^b$). Unlike the common class imbalance caused by the biased dataset, the *fg-bg* imbalance is more likely to be introduced by the “numerous” sample generation strategy. Thus, for a deep object detector, the *fg-bg* imbalance is similarly distributed during training and inference, as the detector always shares the same sample generation strategy in those two phases.

2) *Heuristic Sampling Methods*: Whether hard or soft sampling, the essence is to re-sample or re-weight training samples in the loss computation. If we regard hard sampling as soft sampling with weights 0 or 1, both of them be summarized as

$$L = s \sum_i^N w_i l_i, \quad (1)$$

where L denotes the overall training loss for a batch, and s is a scaling term. w_i and l_i are the weight and the loss of i -th sample in a batch, respectively. In general, deep object detectors uses cross-entropy (CE) loss as l_i in the classification task, *i.e.*

$$L = -s \sum_i^N w_i [y_i \log(p_i) + (1 - y_i) \log(1 - p_i)], \quad (2)$$

where y_i is the ground-truth label for i -th sample: $y_i = 1$ if it is foreground, otherwise $y_i = 0$. p_i is the confidence score, ranging from 0 to 1. Since the weights for foreground and background samples usually have different forms, Equation 2 can be further rewritten as

$$L = -s \sum_i^N w_i^f y_i \log(p_i) + w_i^b (1 - y_i) \log(1 - p_i), \quad (3)$$

where the notations f and b denote foreground and background, respectively. Equation 3 can also describe the training loss without sampling methods. In that case, we have $w_i^f = w_i^b = 1$ for all training samples.

B. Analysis

As most deep object detectors are trained with mini-batch stochastic gradient descent (mini-batch SGD), we discuss here the effect of the *fg-bg* imbalance and heuristic sampling methods on mini-batch SGD training. For each iteration, the learnable parameters Θ of the detector will be updated in the direction of the gradient, *i.e.*

$$\Theta^{t+1} = \Theta^t - \eta \frac{\partial L}{\partial \Theta^t}, \quad (4)$$

where Θ^t denotes the parameters in t step, and η is the learning rate. According to Equation 3, the gradient is

$$\begin{aligned} \frac{\partial L}{\partial \Theta^t} = & -s \sum_i^N y_i g_i \left[\frac{\partial w_i^f}{\partial p_i} \log(p_i) + \frac{w_i^f}{p_i} \right] \\ & + (1 - y_i) g_i \left[\frac{\partial w_i^b}{\partial p_i} \log(1 - p_i) - \frac{w_i^b}{1 - p_i} \right], \end{aligned} \quad (5)$$

where we use g_i to represent $\frac{\partial p_i}{\partial \Theta^t}$, a gradient term between the confidence score and learnable parameters, which is independent of loss and weighting. However, this also means that the exact form of g_i is unknown, thus a quantitative analysis for mini-batch SGD training is impossible. Therefore, we turn to analyze the start and the end of the training phase. Here we only consider the situation of foreground/background classification, which does not involve the bounding-box regression task, to simplify the analysis.

1) *Start of the training*: We denote the learning parameters at the start of the training as Θ_s . At this point, Θ_s cannot distinguish foreground samples from background samples. In other words, the detector outputs similar confidence scores $p_i \approx p$ for all samples. Meanwhile, as we only consider the case of foreground/background classification, the weights can only be set by confidence scores (*e.g.* Focal Loss [17], GHM [24]). Thus, we also have $w_i^f \approx w^f$ and $w_i^b \approx w^b$ due to similar confidence scores. In such a case, the training loss (Equation 3) will be

$$L^{\Theta_s} \approx -s [N^f w^f \log(p) + N^b w^b \log(1 - p)]. \quad (6)$$

According to Equation 5, we can obtain the gradient as

$$\begin{aligned} \frac{\partial L^{\Theta_s}}{\partial \Theta_s} \approx & -s \left\{ \left[\frac{\partial w^f}{\partial p} \log(p) + \frac{w^f}{p} \right] \sum_f g_f \right. \\ & \left. + \left[\frac{\partial w^b}{\partial p} \log(1 - p) - \frac{w^b}{1 - p} \right] \sum_b g_b \right\}, \end{aligned} \quad (7)$$

where the notations f and b denote foreground and background, respectively. Note that at the start of the training, Θ_s is not enough to distinguish different samples. As the parameters are updated, the changes in confidence scores are similar for all samples. That is to say, $g \approx g_i = \frac{\partial p_i}{\partial \Theta_s}$. Thus, Equation 7 can be rewritten as

$$\begin{aligned} \frac{\partial L^{\Theta_s}}{\partial \Theta_s} \approx & -s g \left\{ \left[\frac{\partial w^f}{\partial p} \log(p) + \frac{w^f}{p} \right] N^f \right. \\ & \left. + \left[\frac{\partial w^b}{\partial p} \log(1 - p) - \frac{w^b}{1 - p} \right] N^b \right\}. \end{aligned} \quad (8)$$

If Θ_s is not biased, the initial estimate for both foreground and background samples are $p = 0.5$, then

$$\begin{aligned} \frac{\partial L^{\Theta_s}}{\partial \Theta_s}(p=0.5) &\approx -sg[(2w^f - \frac{\partial w^f}{\partial p} \log 2)N^f \\ &\quad - (2w^b + \frac{\partial w^b}{\partial p} \log 2)N^b]. \end{aligned} \quad (9)$$

When heuristic sampling methods are not used, $w^f = w^b = 1$, then

$$\frac{\partial L^{\Theta_s}}{\partial \Theta_s}(w^f = w^b = 1, p=0.5) \approx -2sg(N^f - N^b). \quad (10)$$

Equation 10 suggests that at the start of the training, the gradient magnitude

$$\left\| \frac{\partial L^{\Theta_s}}{\partial \Theta_s}(w^f = w^b = 1, p=0.5) \right\| \approx 2s|N^f - N^b| \cdot \|g\| \quad (11)$$

of the *fg-bg* imbalance case ($N_f \ll N_b$) will be much larger than that of the balanced case ($N_f \approx N_b$). Thus, if we train a detector without heuristic sampling methods, the *fg-bg* imbalance will result in a much larger gradient magnitude at the start of the training. If the scaling term s is not set properly, it may lead to training divergence. Compared with the gradient magnitude with heuristic sampling methods, the weighting terms $(2w^f - \frac{\partial w^f}{\partial p} \log 2)$ and $(2w^b + \frac{\partial w^b}{\partial p} \log 2)$ can alleviate the imbalance between N_f and N_b . Therefore, heuristic sampling methods will lead to better stability at the start of the training.

However, this does not mean that it is not possible to train the detector without heuristic sampling methods. In fact, we can reduce s to lower the excessive gradient magnitude. But this in turn creates the dilemma of too small gradient magnitude. Specifically, when we set a small s_m as the scaling factor to train a detector without heuristic sampling methods, as $N^f \ll N^b$, p will rapidly approach $p \approx \frac{N^f}{N^f + N^b}$ to achieve a minimal value of $L^{\Theta_s}(w^f = w^b = 1)$, and the gradient magnitude

$$\begin{aligned} \left\| \frac{\partial L^{\Theta_s}}{\partial \Theta_s}(w^f = w^b = 1, s = s_m) \right\| \\ \approx s_m \left| \frac{N^f}{p} - \frac{N^b}{1-p} \right| \cdot \|g\|. \end{aligned} \quad (12)$$

will be greatly decreased. At this point, s_m becomes unreasonable and we should set a large scaling factor. It is not surprising why most effective heuristic sampling methods are dynamic, like Focal Loss [17] and GHM [24].

To sum up, it is essential to control the gradient magnitude in the classification task when training a detector without heuristic sampling methods. As illustrated in [43], [53], the gradient magnitude will have a significant impact on the performance of multi-task learning. Object detection usually

involves two or more tasks, the unreasonable gradient magnitude on the classification task affects not only itself but also other tasks. But in fact, we have various ways to control the gradient magnitude, and the heuristic sampling method is not the only choice.

2) *End of the training*: When we finish training a detector with sampling methods, we will obtain the converged learning parameters Θ^e , which usually leads the training loss to a local minimum. This local minimum may not be globally optimal, but Θ^e often performs well on the classification task. However, it is worth noting that Θ^e only reaches the local minimum of the weighted loss $s \sum_i^N w_i l_i$, rather than the vanilla loss $s \sum_i^N l_i$. Unfortunately, heuristic sampling methods are not available during inference, which means that the “loss function in the inference phase” is likely to be $s \sum_i^N l_i$. From this perspective, it may lead to better classification results without heuristic sampling methods used during training.

Furthermore, the *fg-bg* imbalance, as we illustrated in Sec. III-A, also has the similar distribution in training and inference. If we use heuristic sampling methods during training, then it is equivalent to breaking the consistency of this distribution. In other words, Θ^e is obtained from the weighted imbalance distribution, which may not perform well in the vanilla imbalance distribution. Next, we will experimentally explore how to train deep object detectors without heuristic sampling methods.

C. Experimental Verification

To investigate the accuracy gap between the detector with and without sampling methods, we experimentally investigate the difference between well-known Focal Loss [17] and CE loss. Focal Loss is widely used to address the *fg-bg* imbalance in the one-stage anchor-based and anchor-free object detectors [14], [17], [22], [23], [25]–[33], [40]. In previous studies [17], [24], Focal Loss helps RetinaNet [17] to yield 4~7 higher AP on COCO [44] than CE loss. For simplicity, we denote the RetinaNet with Focal Loss and CE loss as *RetinaNet-FL* and *RetinaNet-CE*, respectively.

There are two differences between *RetinaNet-FL* and *RetinaNet-CE*, one of which is the classification loss. Specifically, *RetinaNet-FL* and *RetinaNet-CE* use Focal Loss (L^{FL}) and CE loss (L^{CE}) in the classification task, respectively. Following the notations in Sec. III-A and Sec. III-B, we have

$$L^{FL} = \frac{1}{N^f} \sum_{i=1}^N w_i l_i, \quad L^{CE} = \frac{1}{N^f} \sum_{i=1}^N l_i, \quad (13)$$

where w_i is an adaptive weighting term. According to [17], an unified representation of weighting term is $\alpha_t(1-p_t)^\gamma$. When we represent it separately for foreground and background samples, we have

$$w_i^f = \alpha(1-p_i)^\gamma, \quad \text{and} \quad w_i^b = (1-\alpha)p_i^\gamma. \quad (14)$$

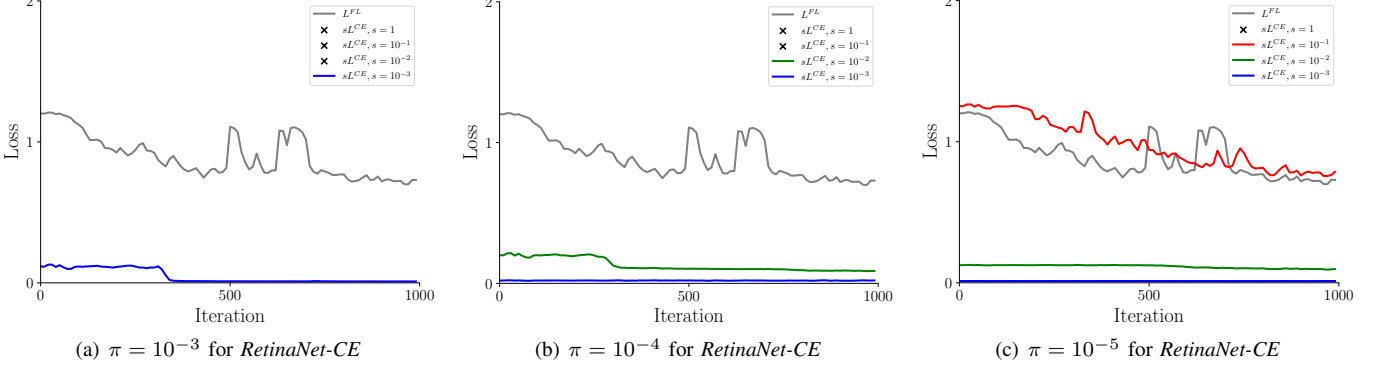


Fig. 2. Loss curves of Focal Loss L^{FL} and cross-entropy loss L^{CE} . “ \times ” means the network diverging. The detector is RetinaNet with ResNet-50-FPN [6], [54] backbone, trained on COCO train2017 [44] with $1\times$ learning schedule [55] (12 epochs), implemented on maskrcnn-benchmark [56]. We only show the first 1k iterations for better visualization.

TABLE I

DETECTION ACCURACY OF *RetinaNet-CE* IN DIFFERENT s AND π ON COCO MINIVAL. “N/A” REFERS TO THE NETWORK DIVERGING.

(a) Accuracy of *RetinaNet-CE* in different π, s

AP	$s = 1$	$s = 10^{-1}$	$s = 10^{-2}$	$s = 10^{-3}$
$\pi = 10^{-2}$	n/a	n/a	n/a	1.6
$\pi = 10^{-3}$	n/a	n/a	n/a	1.6
$\pi = 10^{-4}$	n/a	n/a	26.8	1.6
$\pi = 10^{-5}$	n/a	36.3	26.8	1.6

(b) Accuracy comparison between *RetinaNet-FL* and *RetinaNet-CE*

Model	AP	AP ₅₀	AP ₇₅
<i>RetinaNet-FL</i>	36.4	55.0	39.0
<i>RetinaNet-CE</i> ($\pi = 10^{-5}, s = 10^{-1}$)	36.3	54.8	38.7

Here α and γ are the hyperparameters in Focal Loss for adaptively re-weighting training samples.¹ As Focal Loss uses N^f as the scaling factor, we follow this in CE loss to maintain consistency. However, according to our analysis in Sec. III-B, L^{CE} would lead to an unreasonable gradient magnitude. Therefore, we multiply L^{CE} by a scaling factor of s (sL^{CE}) to reduce the loss scale, as well as reduce the gradient magnitude. We explore how to adjust s in the following.

Another difference between *RetinaNet-FL* and *RetinaNet-CE* is the initialization. Focal Loss uses a biased initialization that initializes the final classification convolutional layer with the bias $b = -\log \frac{1-\pi}{\pi}$. Then, at the start of the training, $p_i = \pi$ is tenable for every training anchor as p_i is computed by sigmoid activation. A heuristic value $\pi = 10^{-2}$ is used in Focal Loss to avoid network diverging. Unfortunately, this will result in network diverging during training *RetinaNet-CE*. We will also explore how to adjust π in the following.

1) *Classification Loss*: Our first discovery is that *RetinaNet-CE* has poor stability on the classification loss, which reflects the unreasonable classification gradient magnitude. This phenomenon corresponds to our discovery in Sec. III-B. Training *RetinaNet-CE* with default $\pi = 10^{-2}$ causes a large classification loss, with the network diverging in a few iterations. See Fig. 2, we observe that *RetinaNet-FL* can be stably trained,

¹We use $\alpha = 0.25, s = 2$ for high detection accuracy, as reported in [17].

but training *RetinaNet-CE* needs to carefully tune π and s to avoid the large classification loss. Only with specific settings, we can obtain several converged models, as shown in Fig. 2.

2) *Detection Accuracy*: Our second discovery is that the classification loss scale will greatly influence the accuracy of the *RetinaNet-CE*. As shown in Table I(a), if a model can be stably trained, then its accuracy will be similar when s is fixed, but tuning s leads to great changes in AP. Table I(b) shows that *RetinaNet-CE* with $\pi = 10^{-5}, s = 10^{-1}$ has already achieved the comparable accuracy of *RetinaNet-FL* (36.3 AP vs. 36.4 AP). This is an inspiring result, as previous works [17], [24] reported there is a 4~7 AP gap between CE loss and Focal Loss. Our investigation successfully narrows this gap. However, it is still unknown why adjusting π and s can help to train *RetinaNet-CE*. Next, we will perform an analysis of this.

3) *Analysis*: At the start of the training, the bias initialization ensures $p_i \approx \pi$ for each training sample. According to Eq. 2, Eq. 13, and Eq. 14, we can estimate L^{FL} as

$$L^{FL} \approx -\alpha(1-\pi)^s \log(\pi) - (1-\alpha)\pi^s \frac{N^b}{N^f} \log(1-\pi), \quad (15)$$

and estimate L^{CE} as

$$sL^{CE} \approx -s \log(\pi) - s \frac{N^b}{N^f} \log(1-\pi). \quad (16)$$

For COCO [44] dataset, a training anchor will learn 80 binary classifiers for 80 object classes. In our observation, the *fg-to-bg* ratio of training anchor is $1 : 10^3$, thus $\frac{N^b}{N^f} \approx 10^3 \times 80$. With $\alpha = 0.25, s = 2, \pi = 10^{-2}$ in training *RetinaNet-FL*, and $s = 10^{-1}, \pi = 10^{-5}$ in training *RetinaNet-CE*, we can estimate L^{FL} and L^{CE} quantitatively as

$$L^{FL} \approx 1.19, \text{ and } L^{CE} \approx 1.23, \quad (17)$$

where the two values are very close. Since the loss scale can reflect the gradient magnitude, we believe that the similar gradient magnitude is the reason for *RetinaNet-CE* with $s = 10^{-1}, \pi = 10^{-5}$ achieves AP comparable to that of *RetinaNet-FL*. Moreover, this setting also facilitates multi-task

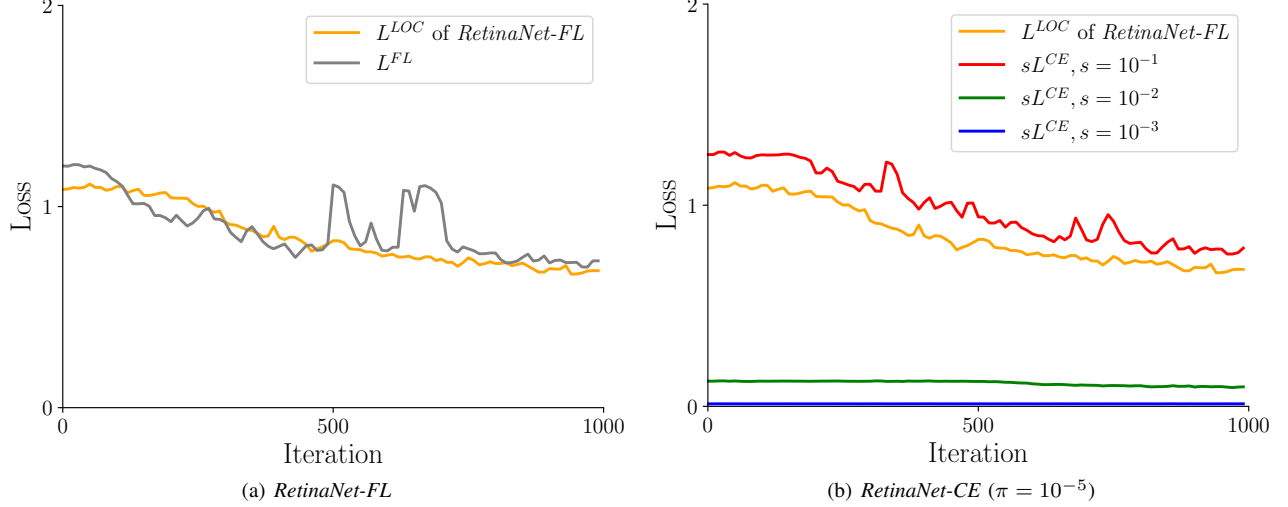


Fig. 3. Loss curves of localization (L^{LOC}) and classification (L^{FL} or L^{CE}), which are from the same models in Fig. 2. Note that the curves of L^{LOC} with different s in (b) are very similar, thus we only show the curve of L^{LOC} with $s = 10^{-1}$ in (b).

learning. See Fig. 3(a), *RetinaNet-FL* achieves a quite good balance between the localization loss L^{LOC} and L^{FL} , whereas Fig. 3(b) shows that only *RetinaNet-CE* with $\pi = 10^{-5}, w = 10^{-1}$ can obtain this balance. Other settings, however, will lead the training to be dominated by the localization task, which is harmful to training an accurate object detector. In conclusion, our investigation reveals that the classification gradient magnitude is the central cause of the accuracy gap, and we can adjust it by initialization and loss scaling.

IV. METHOD

Our investigation reveals that by tuning s and π , the detector without heuristic sampling methods can achieve a similar detection accuracy to that with heuristic sampling methods. However, tuning them is always laborious. In this section, we propose a novel Sampling-Free mechanism, which addresses the *fg-bg* imbalance by adaptively setting s and π , thus adaptively controlling the classification gradient magnitude.

1) *Discarding Heuristic Sampling Methods*: As sampling methods are always a default part in training deep object detectors, the first step of our Sampling-Free mechanism is discarding heuristic sampling methods during training. For one-stage anchor-based object detectors [16]–[23], [40], soft sampling methods (*e.g.* Focal Loss [17], GHM [24], PISA [35]) is widely used for re-weighting training samples in the classification task. In our method, we use the standard CE loss to train the classification task, which treats all training samples equally.

For two-stage anchor-based approaches [4]–[15], hard sampling methods (*e.g.* biased sampling [4], OHEM [34]) are widely used for re-sampling training samples. In our method, we train all training samples in RPN and RoI-subnet. For example, a common implementation of biased sampling [4] in training Faster R-CNN is: (1) RPN randomly selects 256 anchors with a biased 1:1 *fg-to-bg* ratio, (2) RoI-subnet randomly selects 512 proposals with a biased 1:3 *fg-to-bg* ratio. In our method, we train all examples in both RPN and RoI-subnet.

That is to say, we train RPN with all foreground/background anchors ($\sim 10^5$ per-image) and train RoI-subnet with all foreground/background proposals ($\sim 10^3$ per-image). We use CE loss as the classification loss both in RPN and RoI-subnet.

For anchor-free object detectors [11], [14], [25]–[33], they regard “points” as the training samples rather than “anchors” in anchor-based object detectors, and most of them use soft sampling methods to address the *fg-bg* imbalance. We follow the principle of Sampling-Free in anchor-based object detectors that equally use all training samples during training, *i.e.* we use the standard CE loss in the classification task.

2) *Optimal Bias Initialization*: Sec. III-C has shown that adjusting π can help to avoid network diverging. However, it is difficult to determine π . We propose optimal bias initialization to compute π from data statistics rather than tuning it. Our idea is to initialize the bias of the last convolutional layer to obtain a minimal classification loss value. The derivative of L^{CE} is

$$\frac{\partial L^{CE}}{\partial \pi} = -\frac{1}{\pi} + \left(\frac{N}{N^f} - 1\right) \frac{1}{1-\pi}. \quad (18)$$

When $\pi = \frac{N^f}{N}$, $\frac{\partial L^{CE}}{\partial \pi} = 0$, and L^{CE} will attain the minimal value. As the predicted score is predicted with the sigmoid activation, we can obtain the optimal initial bias as

$$b = -\log \frac{1-\pi}{\pi} = -\log \left(\frac{N}{N^f} - 1\right). \quad (19)$$

Here $\frac{N}{N^f}$ can be computed by pre-defined anchors, thus the computation is efficient as it does not require network forwarding. In our observation, $\frac{N}{N^f} \approx 10^5$, which corresponds to $\pi = 10^{-5}$ that performs best in our experiments. It is worth noting that the accuracy of the model is robust to our initialization strategy, as the model can “utilize” the imbalanced distribution to obtain a lower loss. We initialize the model to ensure the stability of the classification loss.

3) *Guided Loss Scaling*: Usually, the overall loss function to train a deep object detector is composed of a localization loss

term and a classification loss term. Let L^t denote the overall loss in the t -th training step. When we use CE loss as the classification loss, we have

$$L^t = (L^{LOC})^t + (L^{CLS})^t = (L^{LOC})^t + s^t (L^{CE})^t, \quad (20)$$

where s^t is used to scale the $(L^{CE})^t$ as the CE loss scale is unreasonable under the $fg\text{-}bg$ imbalance. As mentioned in III-C, it is essential to control the classification loss scale to be close to the localization loss scale. A straightforward way is to adjust s^t . However, it results in a new hyperparameter. Our key idea is to adjust s^t dynamically during training. That says, instead of using a constant s^t , we define a guided term

$$g^t = \frac{(L^{LOC})^t}{(L^{CE})^t}, \quad (21)$$

and let $s^t = g^t$, which suggests to use the localization loss scale of the current mini-batch as the “target” of the rescaled CE loss scale. Thus, this technique is termed guided loss scaling. It is worth noting that g^t is only used for scaling the classification loss, *i.e.* its gradient is ignored in the backpropagation. Therefore, the overall gradient is

$$\frac{\partial L^t}{\partial \Theta^t} = \frac{\partial (L^{LOC})^t}{\partial \Theta^t} + g^t \frac{\partial (L^{CE})^t}{\partial \Theta^t}, \quad (22)$$

which ignores the gradient calculation of s^t .

However, in practice, the detector cannot achieve the best detection accuracy when the classification loss is equal to the localization loss. We introduce a learnable parameter δ^t ($\delta^t > 0$) to learn the best ratio between them (*i.e.* $s^t = g^t \delta^t$), which changes the overall loss to

$$L^t = (L^{LOC})^t + g^t \delta^t (L^{CE})^t - \log \delta^t, \quad (23)$$

where we initialize $\delta^0 = 1$. $-\log \delta^t$ is the normalization term to avoid the degradation of δ^t (*i.e.* $\delta^t \rightarrow 0$). As δ^t is an independent parameter of the detector parameter Θ^t , the overall gradient is changed to

$$\frac{\partial L^t}{\partial \Theta^t} = \frac{\partial (L^{LOC})^t}{\partial \Theta^t} + g^t \delta^t \frac{\partial (L^{CE})^t}{\partial \Theta^t} - \frac{1}{\delta^t}. \quad (24)$$

We observe that the guided term g^t is necessary as δ^t is hard to be learned to make the classification loss and the localization loss to be close. Note that δ is a learnable parameter, it does not need supervision, but only requires an initial value. We use $\delta^0 = 1$ to balance the classification loss and localization loss at the start of the training.

Our guided loss scaling can be interpreted threefold. First, according to Sec. III-C (especially Fig. 3), it appears a good choice to let the localization loss scale and the classification loss scale be similar, where the classification loss is either Focal Loss or CE loss. Second, it is convenient to use the localization loss as guidance, because the localization loss is already there for object detection. Third, the classification loss without sampling methods (*i.e.* CE loss) is greatly influenced by the $fg\text{-}bg$ imbalance, but localization loss is little influenced as it is computed merely for foreground anchors. Thus, the

localization loss is helpful to control the unreasonable classification loss due to the $fg\text{-}bg$ imbalance.

We notice that there have been several works [53], [57], [58] for adaptive multi-task loss scaling. Our guided loss scaling is different from them in three points: 1) it is aimed at controlling the classification loss under the $fg\text{-}bg$ imbalance, which belongs to the single-task loss weighting rather than the multi-task loss weighting; 2) it is specifically designed for deep object detectors as it requires the localization loss to guide the classification loss; 3) it converts the class imbalance problem to the loss scaling problem, which seems not reported before in the literature, to our best knowledge.

V. EXPERIMENTS

In this section, we will perform extensive experiments to validate our Sampling-Free mechanism. Before that, we first describe the experimental details about datasets and baselines. Then, we perform ablation studies of Sampling-Free on anchor-based and anchor-free object detectors. Finally, we compare our Sampling-Free with existing heuristic sampling methods and show the impressive results that our Sampling-Free mechanism achieved.

A. Implementation Details

1) *Datasets*: We use the well-known COCO [44] and PASCAL VOC [45] datasets to validate our method. For COCO dataset, following the common practice [4], [17], we train models on the `train2017` split and perform ablation studies on `minival` split, and report high detection accuracy on `test-dev` split, where COCO-style average precision (AP) is used as the evaluation metrics. For PASCAL VOC dataset, we also follow common practice [4], [20] that training models on a union set of PASCAL VOC 2007 and 2012 set (`07+12` split), and evaluated on PASCAL VOC 2007 test set (`07test` split), where VOC-style mean average precision (mAP) is used as the evaluation metrics.

2) *Baselines*: We use three object detectors — RetinaNet [17] (one-stage anchor-based), Faster R-CNN [4] (two-stage anchor-based), FCOS [31] (anchor-free) that implemented on `maskrcnn-benchmark` [56] to perform experiments, where we follow the public standard training configurations to implement them, which means that we have not made any changes for the hyperparameters of them. Besides, we also use Mask R-CNN [7] to validate Sampling-Free in the instance segmentation task.

B. Ablation Studies

1) *Detection Accuracy*: As shown in Table II, we perform experiments of Sampling-Free on RetinaNet, FCOS, and Faster R-CNN, respectively. See Table II(a) and Table II(b), the experimental phenomena of Sampling-Free on RetinaNet and FCOS are similar. Only when we discard heuristic sampling methods (Focal Loss \rightarrow CE Loss) and use optimal bias initialization with guided loss scaling at the same time, we can obtain meaningful detection accuracy improvements. Specifically, Sampling-Free achieves 0.6 AP and 0.5 AP higher than

TABLE II

ABLATION STUDIES OF OUR SAMPLING-FREE MECHANISM ON COCO MINIVAL. BETTER AP CAN BE ACHIEVED WITH SAMPLING-FREE, BUT THE HYBRID OF THE GUIDED LOSS SCALING AND HEURISTIC SAMPLING METHODS CANNOT IMPROVE THE DETECTION ACCURACY.

(a) Ablation studies of Sampling-Free in RetinaNet [17]

Sampling-Free Mechanism	RetinaNet (ResNet-50-FPN [6], [54], 1×)					
Focal Loss → CE loss	✗	✓	✓	✓	✗	✓
Optimal Bias Initialization	✗	✗	✓	✗	✓	✓
Guided Loss Scaling	✗	✗	✗	✓	✓	✓
AP	36.4	n/a	n/a	n/a	36.5	37.0
AP ₅₀	55.0	n/a	n/a	n/a	55.5	56.5
AP ₇₅	39.0	n/a	n/a	n/a	38.8	39.2
AP _S	19.9	n/a	n/a	n/a	20.1	20.3
AP _M	40.3	n/a	n/a	n/a	40.1	40.5
AP _L	48.9	n/a	n/a	n/a	48.1	49.5

(b) Ablation studies of Sampling-Free in FCOS [31]

Sampling-Free Mechanism	FCOS (ResNet-50-FPN [6], [54], 1×)					
Focal Loss → CE loss	✗	✓	✓	✓	✗	✓
Optimal Bias Initialization	✗	✗	✓	✗	✓	✓
Guided Loss Scaling	✗	✗	✗	✓	✓	✓
AP	37.1	n/a	n/a	n/a	37.1	37.6
AP ₅₀	56.0	n/a	n/a	n/a	56.2	57.4
AP ₇₅	39.8	n/a	n/a	n/a	39.7	40.3
AP _S	21.3	n/a	n/a	n/a	21.0	21.9
AP _M	41.0	n/a	n/a	n/a	41.3	41.2
AP _L	47.8	n/a	n/a	n/a	47.9	48.5

(c) Ablation studies of Sampling-Free in Faster R-CNN [4]

Sampling-Free Mechanism	Faster R-CNN (ResNet-50-FPN [6], [54], 1×)								
	RPN RoI		RPN RoI		RPN RoI		RPN RoI		
Biased Sampling → Non-sampling	✗	✗	✗	✗	✗	✗	✗	✓	
Optimal Bias Initialization + Guided Loss Scaling	✗	✗	✓	✗	✓	✓	✗	✓	
AP	36.8		36.5 (-0.3)		36.4 (-0.4)	36.8 (+0.0)	37.5 (+0.7)	38.1 (+1.3)	38.4 (+1.6)
AP ₅₀	58.4		58.2 (-0.2)		57.9 (-0.5)	58.7 (+0.3)	59.0 (+0.6)	59.6 (+1.2)	59.9 (+1.5)
AP ₇₅	40.0		39.6 (-0.4)		39.4 (-0.6)	40.0 (+0.0)	40.4 (+0.4)	41.6 (+1.6)	41.7 (+1.7)
AP _S	20.7		21.2 (+0.5)		21.1 (+0.4)	21.1 (+0.4)	21.5 (+0.8)	22.2 (+1.5)	22.3 (+1.6)
AP _M	39.7		39.4 (-0.3)		39.1 (-0.6)	40.0 (+0.3)	40.7 (+1.0)	41.2 (+1.5)	41.6 (+1.9)
AP _L	47.9		47.6 (-0.3)		47.5 (-0.4)	47.8 (-0.1)	48.8 (+0.9)	50.0 (+2.1)	50.9 (+3.0)

TABLE III

TRAINING SPEED AND MEMORY COST OF SAMPLING-FREE IN FASTER R-CNN, WHICH IS EVALUATED ON A SINGLE NVIDIA-TITAN-XP GPU WITH BATCH SIZE 1.

Detector	Method	Speed	Memory
Faster R-CNN (ResNet-50-FPN, 1×)	Biased Sampling	172ms	1714MB
	Sampling-Free	184ms	1669MB

Focal Loss in RetinaNet and FCOS, respectively. This is an impressive improvement as the well-known GHM-C [24] only outperforms Focal Loss 0.2 AP. More importantly, this is the first time that CE Loss has achieved better performance than the soft sampling method in object detection.

For Faster R-CNN (See Table II(c)), when we discard heuristic sampling methods without optimal bias initialization and guided loss scaling, the training of the detector will be failed. When we only use the optimal bias initialization and guided loss scaling without discarding heuristic sampling methods, the detector also cannot obtain improvement on detection accuracy. Only when we discard heuristic sampling methods, and use optimal bias initialization with guided loss scaling at the same time, we will observe obvious gains in AP. Sampling-Free improves 0.7 AP and 1.3 AP in RPN and RoI-subnet, respectively. When we use Sampling-Free in both RPN and RoI-subnet, an impressive 1.6 AP improvement can be obtained, with the gains from all AP metrics.

We notice that Sampling-Free exhibits more improvements to Faster R-CNN than RetinaNet and FCOS, which may be due to biased sampling wasting most background examples, but Sampling-Free allows all foreground and background examples to be trained synchronously.

2) *Training Speed and Memory Cost*: As both Focal Loss and Sampling-Free use all samples to train, the training speed and the memory cost of *RetinaNet-FL* and *RetinaNet-CE* are very similar. However, Sampling-Free allows more

TABLE IV

RESULTS OF SAMPLING-FREE ON COCO TEST-DEV.

Detector	Method	AP	AP ₅₀	AP ₇₅
Faster R-CNN (ResNet-101-FPN, 1×)	Biased Sampling	39.3	61.4	42.7
	Sampling-Free	40.7	62.4	44.3
RetinaNet (ResNet-101-FPN, 1×)	Focal Loss	38.8	58.4	41.7
	Sampling-Free	39.4	58.2	42.9
Faster R-CNN (ResNet-101-FPN, 2×)	Biased Sampling	39.6	61.3	43.0
	Sampling-Free	41.0	62.6	44.6
RetinaNet (ResNet-101-FPN, 2×)	Focal Loss	38.9	58.4	41.7
	Sampling-Free	39.5	58.3	43.2

TABLE V
RESULTS OF SAMPLING-FREE ON PASCAL VOC 07 TEST SPLIT.

Detector	Method	mAP
RetinaNet (ResNet-50-FPN, 0.2×)	Focal Loss	79.3
	Sampling-Free	80.1
Faster R-CNN (ResNet-50-FPN, 0.2×)	Biased Sampling	80.9
	Sampling-Free	81.5

background samples to be trained than biased sampling, thus we discuss the training speed and memory cost of Sampling-Free in Faster R-CNN. As shown in Table III, we measure the performance of Faster R-CNN with Sampling-Free on a single Nvidia-Titan-Xp GPU with batch size 1. Interestingly, although the training speed becomes slower for Faster R-CNN with Sampling-Free (as more background proposals are trained in RoI-subnet), its memory cost is reduced, which is owing to the operation of biased sampling also requires considerable memory costs.

C. Experimental Results

1) *Results on COCO and PASCAL VOC*: For COCO dataset, we have demonstrated that the effectiveness of Sampling-Free on ResNet-50-FPN backbone and 1× learning schedule. We further verify our methods on the larger backbone and the

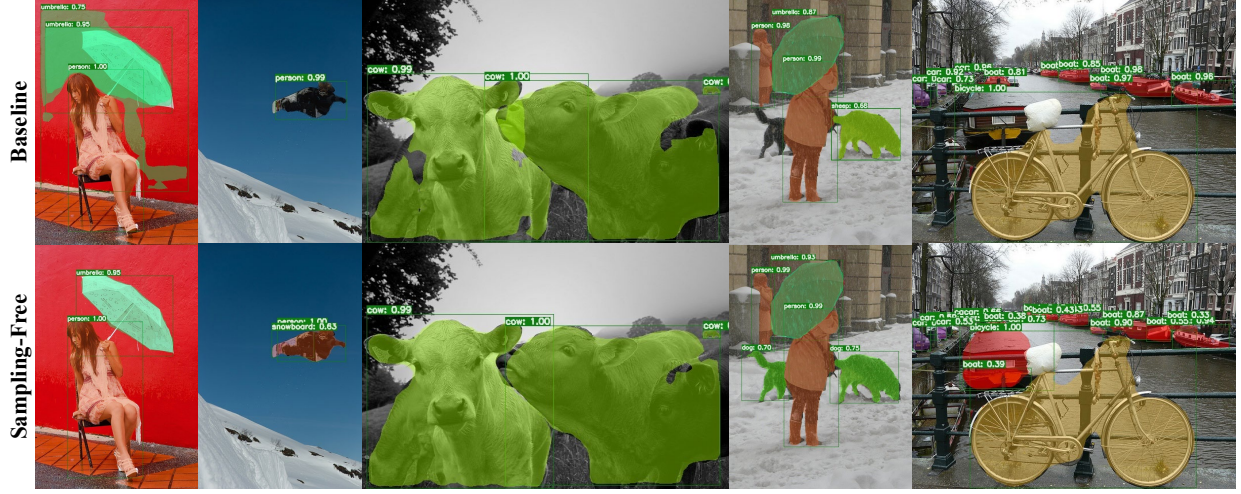


Fig. 4. Mask R-CNN [7] (37.8 box AP, 34.2 mask AP on COCO minival) vs. Mask R-CNN with Sampling-Free (39.0 box AP, 34.9 mask AP on COCO minival) in ResNet-50-FPN backbone. The latter exhibits better detection and segmentation results.

TABLE VI

RESULTS OF ADAPTIVE LABEL ASSIGNMENT STRATEGIES WITH OUR SAMPLING-FREE MECHANISM.

(a) AP of ATSS (ResNeXt-64x4d-101-DCN, 2 \times) on COCO test-dev

Method	AP	AP ₅₀	AP ₇₅	AP _S	AP _M	AP _L
ATSS [38]	47.7	66.5	51.9	29.7	50.8	59.4
w. Sampling-Free	48.2	66.9	52.4	30.3	51.3	59.9

(b) AP of PAA (ResNeXt-64x4d-101-DCN, 2 \times) on COCO test-dev

Method	AP	AP ₅₀	AP ₇₅	AP _S	AP _M	AP _L
PAA [39]	49.0	67.8	53.3	30.2	52.8	62.2
w. Sampling-Free	49.6	68.3	53.8	30.6	53.7	63.1

TABLE VII

RESULTS OF SAMPLING-FREE IN THE INSTANCE SEGMENTATION TASK.

(a) Box AP of Mask R-CNN (ResNet-50-FPN, 1 \times) on COCO minival split

Method	AP	AP ₅₀	AP ₇₅	AP _S	AP _M	AP _L
Mask R-CNN [7]	37.8	59.3	41.1	21.5	41.1	49.9
w. Sampling-Free	39.0	60.3	42.5	22.5	41.9	51.2

(b) Mask AP of Mask R-CNN (ResNet-50-FPN, 1 \times) on COCO minival split

Method	AP	AP ₅₀	AP ₇₅	AP _S	AP _M	AP _L
Mask R-CNN [7]	34.2	55.9	36.3	15.6	36.8	50.6
w. Sampling-Free	34.9	56.8	37.1	16.2	37.3	51.2

longer learning schedule. As shown in Table IV, for ResNet-101-FPN backbone, Sampling-Free still shows impressive detection accuracy improvements, which can improve Faster R-CNN and RetinaNet about 1.5 AP and 0.5 AP, respectively. Even with the 2 \times learning schedule, we observe a steady increase in AP as well.

For PASCAL VOC dataset, as shown in Table V, Sampling-Free improves 0.8 mAP and 0.6 mAP for RetinaNet and Faster R-CNN, respectively. These results illustrate the robustness of our Sampling-Free mechanism.

2) *Results on Adaptive Label Assignment Strategies*: To date, the state-of-the-art detection accuracy is achieved by adaptive label assignment methods, where the definition of foreground/background training sample is very different from that in deep object detectors. To validate the effectiveness of Sampling-Free in them, we replace Focal Loss with Sampling-Free in ATSS [38] and PAA [39]. As presented in Table VI, we successfully verify that the state-of-the-art models of ATSS and PAA can be further improved with Sampling-Free.

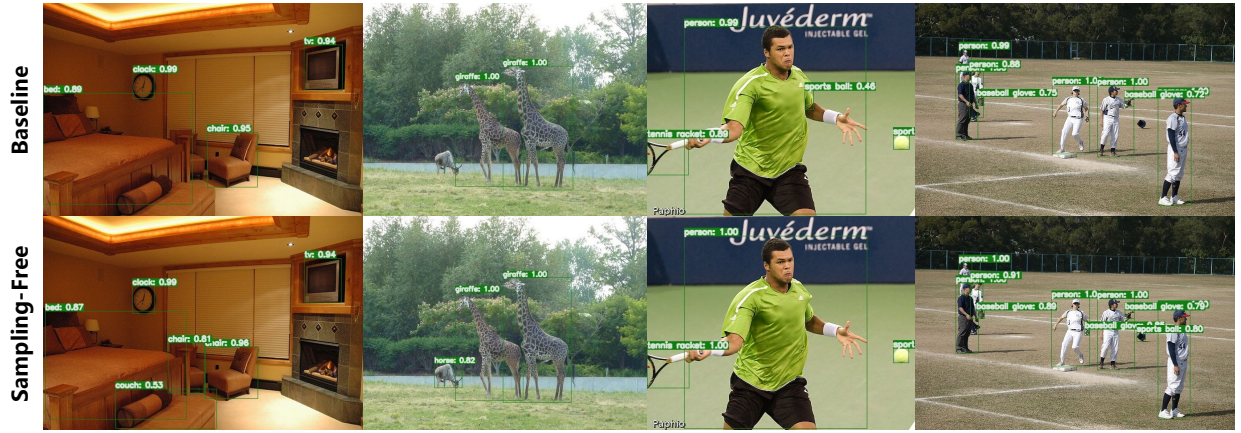
3) *Instance Segmentation*: Although Sampling-Free can help detectors achieve better detection accuracy, it is unknown whether detection results produced with Sampling-Free mechanism can facilitate other tasks in practice. Therefore, we introduce Sampling-Free into Mask R-CNN to observe whether it can achieve higher accuracy in instance segmentation. Note that in Mask R-CNN, the heuristic sampling method is not used in its segmentation branch, thus we only apply our Sampling-Free mechanism on the classification branch. As shown in Table VII, Mask R-CNN with Sampling-Free achieves 1.2 box AP and 0.7 mask AP gains. We visualize the detection and segmentation results in Fig. 5, which suggests that the detection results produced with Sampling-Free can also improve the instance segmentation task.

4) *Comparison*: We compare Sampling-Free with existing heuristic sampling methods to illustrate our advantages. As the implementations of Sampling-Free and other methods may be on different platforms (e.g. maskrcnn-benchmark [56] vs. mmdetection [59]), we mainly compare their changes in performance relative to the baseline method (Focal Loss in RetinaNet, Biased Sampling in Faster R-CNN). As presented in Table VIII, compared with heuristic sampling methods, Sampling-Free has the following three advantages:

- Sampling-Free achieves the best relative detection accuracy improvement, where 0.6 AP and 1.6 AP improvement are obtained in RetinaNet and Faster R-CNN, respectively.
- Sampling-Free has no hyperparameters to search — In contrast, other heuristic sampling methods has at least one hyperparameter. The ISR [35], which is closest to us in



(a) RetinaNet with our Sampling-Free mechanism exhibits better performance than RetinaNet with Focal Loss (baseline).



(b) Faster R-CNN with our Sampling-Free mechanism exhibits better performance than Faster R-CNN with biased sampling (baseline).

Fig. 5. Detection results of object detectors with and without our Sampling-Free mechanism. The backbone of these detectors is ResNet-50-FPN [6], [54].

TABLE VIII

THIS TABLE ILLUSTRATES THE COMPARISON BETWEEN HEURISTIC SAMPLING METHODS AND OUR SAMPLING-FREE MECHANISM. ΔAP AND Δ HYPERPARAMETERS DENOTE THE CHANGE IN DETECTION ACCURACY AND HYPERPARAMETERS RELATIVE TO THE BASELINE METHOD (FOCAL LOSS IN RETINANET, BIASED SAMPLING IN FASTER R-CNN). SAMPLING-FREE ACHIEVES THE BEST ΔAP IN BOTH RETINANET AND FASTER R-CNN, WITHOUT ANY HYPERPARAMETER INTRODUCED.

Solutions	Abbreviation	ΔAP in RetinaNet (ResNet-50-FPN, 1 \times)	ΔAP in Faster R-CNN (ResNet-50-FPN, 1 \times)	Δ hyperparameters
Hard Sampling	OHEM [34]	n/a	36.4 \rightarrow 36.6 (+0.2 AP)	2 \rightarrow 2
	IoU-balanced sampling [12]	n/a	36.4 \rightarrow 36.8 (+0.4 AP)	2 \rightarrow 3
Soft Sampling	GHM-C [24]	35.6 \rightarrow 35.8 (+0.2 AP)	n/a	2 \rightarrow 1
	ISR [35]	n/a	36.4 \rightarrow 37.9 (+1.5 AP)	2 \rightarrow 4
Non-Sampling	Sampling-Free	36.4 \rightarrow 37.0 (+0.6 AP)	36.8 \rightarrow 38.4 (+1.6 AP)	2 \rightarrow 0

detection accuracy, introduces 4 hyperparameters.

- Sampling-Free has better versatility — it is applicable to both one-stage and two-stage deep object detectors.

5) *Visualization:* More visualization results are in Fig. 5.

VI. CONCLUSION

In this paper, we explored whether heuristic sampling methods are necessary for training accurate deep object detectors under the *fg-bg* imbalance. Our investigation revealed that the key to training without heuristic sampling methods under the *fg-bg* imbalance is to control the classification gradient magnitude. Inspired by this, we proposed a novel Sampling-Free mechanism to control the classification gradient magni-

tude from initialization and loss scaling, without new hyperparameters introduced. Extensive experiments demonstrated the effectiveness of Sampling-Free in various object detectors, which also yields considerable gains in the instance segmentation task and the state-of-the-art label assignment strategies. Our Sampling-Free mechanism provides a new perspective to address the *fg-bg* imbalance.

Although Sampling-Free can support training with cross-entropy loss, it is not designed for the detection metrics, which may limit further performance increases. Specifically, the average precision metric expects samples to have an IoU-related confidence score. There has been some work on this [60], [61], but they still use a variant of Focal Loss to train the classification task. Thus, a future study is to use only

cross-entropy loss to model this unified confidence score. On a larger scale, one can try to use cross-entropy loss with metric-specific design to achieve better performance.

REFERENCES

- [1] A. Krizhevsky, I. Sutskever, and G. E. Hinton, “Imagenet classification with deep convolutional neural networks,” *Commun. ACM*, vol. 60, no. 6, pp. 84–90, 2017.
- [2] Y. LeCun, Y. Bengio, and G. E. Hinton, “Deep learning,” *Nature*, vol. 521, no. 7553, pp. 436–444, 2015.
- [3] L. Liu, W. Ouyang, X. Wang, P. Fieguth, J. Chen, X. Liu, and M. Pietikäinen, “Deep learning for generic object detection: A survey,” *IJCV*, pp. 1573–1405, 2019.
- [4] S. Ren, K. He, R. B. Girshick, and J. Sun, “Faster R-CNN: towards real-time object detection with region proposal networks,” *TPAMI*, vol. 39, no. 6, pp. 1137–1149, 2017.
- [5] J. Dai, Y. Li, K. He, and J. Sun, “R-FCN: object detection via region-based fully convolutional networks,” in *NIPS*, 2016, pp. 379–387.
- [6] T. Lin, P. Dollár, R. B. Girshick, K. He, B. Hariharan, and S. J. Belongie, “Feature pyramid networks for object detection,” in *CVPR*, 2017, pp. 936–944.
- [7] K. He, G. Gkioxari, P. Dollár, and R. B. Girshick, “Mask R-CNN,” in *ICCV*, 2017, pp. 2980–2988.
- [8] H. Hu, J. Gu, Z. Zhang, J. Dai, and Y. Wei, “Relation networks for object detection,” in *CVPR*, 2018, pp. 3588–3597.
- [9] Z. Cai and N. Vasconcelos, “Cascade R-CNN: delving into high quality object detection,” in *CVPR*, 2018, pp. 6154–6162.
- [10] B. Jiang, R. Luo, J. Mao, T. Xiao, and Y. Jiang, “Acquisition of localization confidence for accurate object detection,” in *ECCV*, 2018, pp. 816–832.
- [11] X. Lu, B. Li, Y. Yue, Q. Li, and J. Yan, “Grid R-CNN,” in *CVPR*, 2019, pp. 7363–7372.
- [12] J. Pang, K. Chen, J. Shi, H. Feng, W. Ouyang, and D. Lin, “Libra R-CNN: towards balanced learning for object detection,” in *CVPR*, 2019, pp. 821–830.
- [13] K. Chen, J. Pang, J. Wang, Y. Xiong, X. Li, S. Sun, W. Feng, Z. Liu, J. Shi, W. Ouyang, C. C. Loy, and D. Lin, “Hybrid task cascade for instance segmentation,” in *CVPR*, 2019, pp. 4974–4983.
- [14] J. Wang, K. Chen, S. Yang, C. C. Loy, and D. Lin, “Region proposal by guided anchoring,” in *CVPR*, 2019, pp. 2965–2974.
- [15] Y. Li, Y. Chen, N. Wang, and Z. Zhang, “Scale-aware trident networks for object detection,” in *ICCV*, 2019, pp. 6054–6063.
- [16] T. Kong, F. Sun, A. Yao, H. Liu, M. Lu, and Y. Chen, “RON: reverse connection with objectness prior networks for object detection,” in *CVPR*, 2017, pp. 5244–5252.
- [17] T. Lin, P. Goyal, R. B. Girshick, K. He, and P. Dollár, “Focal loss for dense object detection,” in *ICCV*, 2017, pp. 2999–3007.
- [18] J. Redmon and A. Farhadi, “YOLO9000: better, faster, stronger,” in *CVPR*, 2017, pp. 6517–6525.
- [19] ———, “Yolov3: An incremental improvement,” *arXiv:1804.02767*, 2018.
- [20] S. Zhang, L. Wen, X. Bian, Z. Lei, and S. Z. Li, “Single-shot refinement neural network for object detection,” in *CVPR*, 2018, pp. 4203–4212.
- [21] S. Liu, D. Huang, and Y. Wang, “Receptive field block net for accurate and fast object detection,” in *ECCV*, 2018, pp. 404–419.
- [22] C. Zhu, Y. He, and M. Savvides, “Feature selective anchor-free module for single-shot object detection,” in *CVPR*, 2019, pp. 840–849.
- [23] X. Zhang, F. Wan, C. Liu, R. Ji, and Q. Ye, “Freearchor: Learning to match anchors for visual object detection,” in *NeurIPS*, 2019, pp. 147–155.
- [24] B. Li, Y. Liu, and X. Wang, “Gradient harmonized single-stage detector,” in *AAAI*, 2019, pp. 8577–8584.
- [25] H. Law and J. Deng, “Cornernet: Detecting objects as paired keypoints,” in *ECCV*, 2018, pp. 765–781.
- [26] X. Zhou, J. Zhuo, and P. Krähenbühl, “Bottom-up object detection by grouping extreme and center points,” in *CVPR*, 2019, pp. 850–859.
- [27] X. Zhou, D. Wang, and P. Krähenbühl, “Objects as points,” *arXiv:1904.07850*, 2019.
- [28] K. Duan, S. Bai, L. Xie, H. Qi, Q. Huang, and Q. Tian, “Centernet: Keypoint triplets for object detection,” in *ICCV*, 2019, pp. 6569–6578.
- [29] Z. Yang, S. Liu, H. Hu, L. Wang, and S. Lin, “Reppoints: Point set representation for object detection,” in *ICCV*, 2019, pp. 9657–9666.
- [30] Z. Yang, Y. Xu, H. Xue, Z. Zhang, R. Urtasun, L. Wang, S. Lin, and H. Hu, “Dense reppoints: Representing visual objects with dense point sets,” in *ECCV*, 2020.
- [31] Z. Tian, C. Shen, H. Chen, and T. He, “FCOS: fully convolutional one-stage object detection,” in *ICCV*, 2019, pp. 9627–9636.
- [32] T. Kong, F. Sun, H. Liu, Y. Jiang, L. Li, and J. Shi, “Foveabox: Beyond anchor-based object detector,” *TIP*, pp. 7389–7398, 2020.
- [33] C. Zhu, F. Chen, Z. Shen, and M. Savvides, “Soft anchor-point object detection,” in *ECCV*, 2020.
- [34] A. Shrivastava, A. Gupta, and R. B. Girshick, “Training region-based object detectors with online hard example mining,” in *CVPR*, 2016, pp. 761–769.
- [35] Y. Cao, K. Chen, C. C. Loy, and D. Lin, “Prime sample attention in object detection,” in *CVPR*, 2020, pp. 11 583–11 591.
- [36] K. Oksuz, B. C. Cam, S. Kalkan, and E. Akbas, “Imbalance problems in object detection: A review,” *TPAMI*, pp. 1–1, 2020.
- [37] H. Li, Z. Wu, C. Zhu, C. Xiong, R. Socher, and L. S. Davis, “Learning from noisy anchors for one-stage object detection,” in *CVPR*, 2020, pp. 10 585–10 594.
- [38] S. Zhang, C. Chi, Y. Yao, Z. Lei, and S. Z. Li, “Bridging the gap between anchor-based and anchor-free detection via adaptive training sample selection,” in *CVPR*, 2020, pp. 9756–9765.
- [39] K. Kim and H. S. Lee, “Probabilistic anchor assignment with iou prediction for object detection,” in *ECCV*, 2020.
- [40] W. Ke, T. Zhang, Z. Huang, Q. Ye, J. Liu, and D. Huang, “Multiple anchor learning for visual object detection,” in *Proceedings of the IEEE/CVF Conference on Computer Vision and Pattern Recognition (CVPR)*, June 2020, pp. 10 206–10 215.
- [41] K. Chen, J. Li, W. Lin, J. See, J. Wang, L. Duan, Z. Chen, C. He, and J. Zou, “Towards accurate one-stage object detection with ap-loss,” in *CVPR*, 2019, pp. 5119–5127.
- [42] Q. Qian, L. Chen, H. Li, and R. Jin, “DR loss: Improving object detection by distributional ranking,” in *CVPR*, 2020, pp. 12 161–12 169.
- [43] K. Oksuz, B. C. Cam, E. Akbas, and S. Kalkan, “A ranking-based, balanced loss function unifying classification and localisation in object detection,” in *NeurIPS*, 2020.
- [44] T. Lin, M. Maire, S. J. Belongie, J. Hays, P. Perona, D. Ramanan, P. Dollár, and C. L. Zitnick, “Microsoft COCO: common objects in context,” in *ECCV*, 2014, pp. 740–755.
- [45] M. Everingham, L. J. V. Gool, C. K. I. Williams, J. M. Winn, and A. Zisserman, “The pascal visual object classes (VOC) challenge,” *IJCV*, vol. 88, no. 2, pp. 303–338, 2010.
- [46] P. F. Felzenszwalb, R. B. Girshick, and D. A. McAllester, “Cascade object detection with deformable part models,” in *CVPR*, 2010, pp. 2241–2248.
- [47] P. A. Viola and M. J. Jones, “Robust real-time face detection,” *IJCV*, vol. 57, no. 2, pp. 137–154, 2004.
- [48] R. B. Girshick, J. Donahue, T. Darrell, and J. Malik, “Rich feature hierarchies for accurate object detection and semantic segmentation,” in *CVPR*, 2014, pp. 580–587.
- [49] R. B. Girshick, “Fast R-CNN,” in *ICCV*, 2015, pp. 1440–1448.
- [50] W. Liu, D. Anguelov, D. Erhan, C. Szegedy, S. E. Reed, C. Fu, and A. C. Berg, “SSD: single shot multibox detector,” in *ECCV*, 2016, pp. 21–37.
- [51] K. Oksuz, B. C. Cam, E. Akbas, and S. Kalkan, “Generating positive bounding boxes for balanced training of object detectors,” in *WACV*, 2020, pp. 883–892.
- [52] X. Wang, A. Shrivastava, and A. Gupta, “A-fast-rcnn: Hard positive generation via adversary for object detection,” in *CVPR*, 2017, pp. 3039–3048.
- [53] Z. Chen, V. Badrinarayanan, C. Lee, and A. Rabinovich, “Gradnorm: Gradient normalization for adaptive loss balancing in deep multitask networks,” in *ICML*, 2018, pp. 793–802.
- [54] K. He, X. Zhang, S. Ren, and J. Sun, “Deep residual learning for image recognition,” in *CVPR*, 2016, pp. 770–778.
- [55] R. Girshick, I. Radosavovic, G. Gkioxari, P. Dollár, and K. He, “Detectron,” 2018. [Online]. Available: <https://github.com/facebookresearch/detectron>
- [56] M. Francisco and G. Ross, “maskrcnn-benchmark,” 2018. [Online]. Available: <https://github.com/facebookresearch/maskrcnn-benchmark>
- [57] A. Kendall, Y. Gal, and R. Cipolla, “Multi-task learning using uncertainty to weigh losses for scene geometry and semantics,” in *CVPR*, 2018, pp. 7482–7491.
- [58] O. Sener and V. Koltun, “Multi-task learning as multi-objective optimization,” in *NeurIPS*, 2018, pp. 525–536.
- [59] K. Chen, J. Wang, J. Pang, Y. Cao, Y. Xiong, X. Li, S. Sun, W. Feng, Z. Liu, J. Xu, Z. Zhang, D. Cheng, C. Zhu, T. Cheng, Q. Zhao, B. Li, X. Lu, R. Zhu, Y. Wu, J. Dai, J. Wang, J. Shi, W. Ouyang, C. C. Loy, and D. Lin, “Mmdetection: Open mmlab detection toolbox and benchmark,” *arXiv:1906.07155*, 2019.

- [60] H. Zhang, Y. Wang, F. Dayoub, and N. Sünderhauf, “Varifocalnet: An iou-aware dense object detector,” in *CVPR*, 2021.
- [61] X. Li, W. Wang, L. Wu, S. Chen, X. Hu, J. Li, J. Tang, and J. Yang, “Generalized focal loss: Learning qualified and distributed bounding boxes for dense object detection,” in *NeurIPS*, 2020.